Flow of a viscous fluid past a flexible membrane at low Reynolds numbers

1992 Fluid Dyn. Res. 9 289

(http://iopscience.iop.org/1873-7005/9/5-6/A06)

Fluid Dynamics Research 9 (1992) 289–299
North-Holland

FLUID DYNAMICS RESEARCH

Flow of a viscous fluid past a flexible membrane at low Reynolds numbers

Kyoji Yamamoto, Makoto Okada and Jun-ichi Kameyama

Department of Mechanical Engineering, Faculty of Engineering, Okayama University, Okayama 700, Japan

Received 4 December 1990

Abstract. The numerical calculation of a steady two-dimensional viscous flow past a flexible membrane is treated. Both edges of the membrane are fixed in the flow and its chord is set normal to the flow. The Navier–Stokes equation in terms of the stream function and the vorticity is transformed to the body fitted coordinate system. The numerical calculations, based on a finite difference method and relaxation method, are carried out for several values of the membranes tension for cases when the Reynolds numbes are 5, 10 and 20. It is found that two different shapes of the membranes are possible at a given value of tension and Reynolds number: one with a small deformation, and the other with a large deformation. Two vortices appear in the concave region of the membrane if its deformation increases beyond a certain extent.

1. Introduction

One of the interesting and important problems in fluid dynamics is the interaction between the flow and the body. If the body is flexible and hence easily deformable, the shape of the body will be dependent on the viscous and pressure forces generated by the fluid motion; conversely, the load distributions at the body surface depend on the body shape. The shape and the load distribution are determined simultaneously.

Such a situation commonly arises in flows containing bubbles or droplets of liquid, flows with free surfaces, flow past a sail, etc. Zahalak, Rao and Sutera (1987) studied the steady two-dimensional shear flow fields inside and outside an extensible cylindrical membrane assuming the Reynolds number to be zero. This problem is somewhat related to the phenomenon in red blood cells. Youngren and Acrivos (1976) studied the shape of a gas bubble in a viscous extensional flow. The shape of an axisymmetric bubble or drop in a uniform flow was treated by Miksis, Vanden-Broeck and Keller (1981). These studies are based on the so-called boundary-integral technique, which is not restricted to small deformation of the shape, but is restricted to creeping or potential flow. Ryskin and Leal (1984) developed a numerical method based on a finite difference scheme incorporating a numerically generated orthogonal coordinate system, and analyzed the large deformation of an axisymmetric bubble in a flow of intermediate Reynolds numbers. Shanks (1977) carried out a numerical simulation of viscous flow about submerged arbitrary hydrofoils using a finite difference technique. The motion of a sphere in the presence of a deformable interface was studied by Lee and Leal (1982). The shape of the sail may be the most typical example of the deformable body-flow interaction. Thwaites (1961), Nielsen (1963), and Sugimoto and Sato (1988) studied the aerodynamic characteristics of a sail in a steady flow, and found the sail had mutlimodal shapes at a given angle of attack. The stability of the sail shape was investigated by Yamamoto and Ishimaru (1988) in connection with the multimodal shapes in a steady flow. Another interesting deformable body problem may be found in the production

process of polyethylene membrane. When a long sheet of the membrane is wound into a roll, the moving flat sheet is sometimes given a concave or convex shape by a very weak cross wind.

In the present study, as a simple basic flow containing a deformable body, we shall consider a viscous flow past a flexible two-dimensional membrane set normal to the uniform flow and fixed at its ends in the flow. Numerical calculations are carried out when the Reynolds numbers are 5, 10 and 20 for given values of the membrane tension at its fixed ends. The finite difference equations for the vorticity–stream function formulation incorporating a numerically generated boundary fitted coordinates system, which was proposed by Thompson, Thames and Mastin (1974), are solved for an initially assumed shape of the membrane using a relaxation method. The steady shape is determined via an iterative procedure so that the balance of forces at a membrane element may be attained. The flow patterns and the drag acting on the membrane are obtained.

2. Fundamental equations

2.1. Equations for the vorticity and the stream function

We shall take a flexible membrane in a uniform flow of speed U. Let the chord of the membrane be set normal to the uniform flow and the chord length be L. The fundamental equations governing the two-dimensional flow may be written as

$$\omega_t + \psi_y \omega_x - \psi_x \omega_y = (\omega_{xx} + \omega_{yy})/\mathrm{Re}, \tag{2.1}$$

$$\psi_{xx} + \psi_{yy} = -\omega, \tag{2.2}$$

in terms of the vorticity ω and the stream function ψ, where time t, the Cartesian coordinates (x, y), ω, and ψ are non-dimensional quantities given by

$$t = (U/L)t^*, \quad (x, y) = (x^*, y^*)/L,$$
$$\omega = (L/U)\omega^*, \quad \psi = \psi^*/LU, \quad \boldsymbol{u} = \boldsymbol{u}^*/U. \tag{2.3}$$

Here and below, the variables with asterisks are dimensional quantities. Further, Re is the Reynolds number defined by

$$\mathrm{Re} = UL/\nu, \tag{2.4}$$

where ν is the kinematic viscosity. The velocity $\boldsymbol{u} = (u, v)$ is related to the stream function and the vorticity as

$$u = \psi_y, \quad v = -\psi_x, \tag{2.5}$$

$$\omega = v_x - u_y. \tag{2.6}$$

The flow is uniform and parallel to the x-axis at infinity. Therefore, we have

$$\psi \to y, \quad \omega \to 0 \quad \text{as } |\boldsymbol{x}| \to \infty. \tag{2.7}$$

The condition at the membrane surface is given by

$$v_{\mathrm{N}} = \psi = 0, \quad v_{\mathrm{T}} = 0, \tag{2.8}$$

where v_{T} and v_{N} are the velocities tangential and normal to the surface, respectively. We do not know beforehand the membrane shape in equilibrium. We first assume a suitable shape and an initial flow. The shape is changed as time advances so that the balance of forces acting on a small portion of the membrane may be attained. The forces will be balanced in a steady state, and the final shape will be determined.

2.2. Body-fitted coordinates

It is convenient in numerical claculations to introduce a body-fitted coordinate system (ξ, η) given by

$$\xi = \xi(x, y), \quad \eta = \eta(x, y), \tag{2.9}$$

where η = const., say η_1, coincides with the body surface C_1 and $\eta = \eta_2$ represents the outer boundary C_3 to be taken far away from the body. Further, the lines of $\xi = \xi_1$ and $\xi = \xi_2$ coincide with the curves C_4 and C_2, respectively (see fig. 1). This transformation maps the region D bounded by the contour C_1–C_2–C_3–C_4 in the x–y plane onto the rectangular region D′ surrounded by the corresponding contour C_1'–C_2'–C_3'–C_4' in the ξ–η plane. The transformation (2.9) may be obtained by solving the Poisson equation (Thompson et al., 1974):

$$\xi_{xx} + \xi_{yy} = P, \quad \eta_{xx} + \eta_{yy} = Q, \tag{2.10}$$

where P and Q are given functions of ξ and η. Equations (2.10) are to be solved with the boundary conditions that the curves $\eta = \eta_1$ coincides with the membrane surface and the curve $\eta = \eta_2$ represents the outer boundary far from the membrane. The numerical calculation of eqs. (2.1) and (2.2) is to be made in the region $\eta_1 \le \eta \le \eta_2$ and $\xi_1 \le \xi \le \xi_2$. The region of the actual calculation in the ξ–η plane is taken in such a way that $1 \le \xi \le i_{\max}$ and $1 \le \eta \le j_{\max}$, where $i_{\max}$ and $j_{\max}$ are shown in table 1. One of the typical coordinate systems used in the numerical calculation is illustrated in fig. 2. Figure 2a shows the whole domain of the calculation, whereas fig 2b is an enlargement of the coordinate system near the membrane. Using the transformation (2.9), we can rewrite the fundamental equations (2.1) and (2.2), but we do not show their explicit forms for shortness.

2.3. Forces acting on a membrane element

The membrane is fixed at both ends. It is flexible and inextensible so that it may be easily deformed by action of fluid forces. The shape of the membrane in equilibrium in a steady flow can be obtained by considering the balance of the forces acting on a membrane element. If $\boldsymbol{S}$ is the force of fluid per unit area acting on a surface element, then it can be written as

$$\boldsymbol{S} = \sqrt{1/\gamma}\left[py_\xi - (\omega/\mathrm{Re})x_\xi\right]\boldsymbol{i} - \sqrt{1/\gamma}\left[px_\xi + (\omega/\mathrm{Re})y_\xi\right]\boldsymbol{j}, \tag{2.11}$$

$$\gamma = x_\xi^2 + y_\xi^2, \tag{2.12}$$

after using the continuity equation and the non-slip condition at the surface. Here, $\boldsymbol{i}$ and $\boldsymbol{j}$

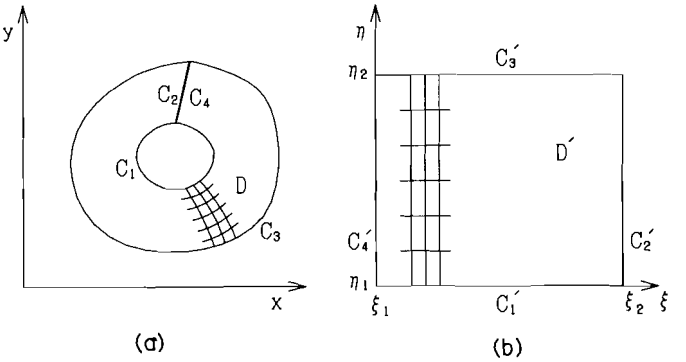

Fig. 1. Field transformation. (a) Physical plane. (b) Transformed plane.

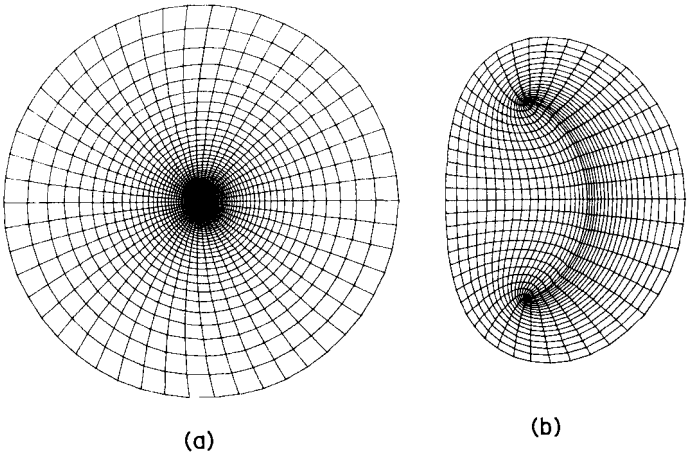

Fig. 2. A typical coordinate system. (a) Whole calculation domain. (b) Region near the membrane.

are the unit vectors in the direction of x and y, respectively, and p is the pressure defined by

$$p = p^*/\rho U^2, \tag{2.13}$$

where ρ is the density of the fluid. It is easy to derive the unit vectors normal ($\boldsymbol{n}$) and tangential ($\boldsymbol{t}$) to the surface. These are given by

$$\boldsymbol{n} = \sqrt{1/\gamma}\,(-y_\xi \boldsymbol{i} + x_\xi \boldsymbol{j}), \quad \boldsymbol{t} = \sqrt{1/\gamma}\,(x_\xi \boldsymbol{i} + y_\xi \boldsymbol{j}). \tag{2.14}$$

From eqs. (2.11) and (2.14) the stresses normal and tangential to the membrane element are given by

$$S_N = -p, \quad S_T = -\omega/\mathrm{Re}. \tag{2.15}$$

Figure 3 shows the system of surface forces on the element. The tangential force acting on the element should be zero if the membrane is in equilibrium. Therefore, we have

$$\mathrm{d}T = (1/\mathrm{Re})(\omega_+ - \omega_-)\,\mathrm{d}s, \tag{2.16}$$

where T is the nondimensional tension of the membrane defined by

$$T = T^*/\rho U^2 L, \tag{2.17}$$

and subscripts + and − denote the values on the downstream- and upstream-sides of the

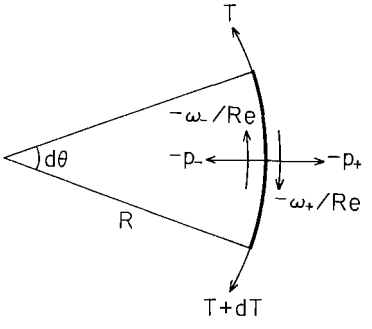

Fig. 3. Forces acting on a membrane element.

membranes, respectively. Further, s is the coordinate along the membrane and ds is related to $d\xi$ by

$$ds = \sqrt{\gamma}\, d\xi. \tag{2.18}$$

Since the net force normal to the membrane element should be zero in equilibrium, we have

$$F \equiv (p_- - p_+)R - T = 0, \tag{2.19}$$

where R is the radius of curvature of the membrane. If the membrane shape is not in equilibrium, the normal force

$$\boldsymbol{F} \equiv F\boldsymbol{n} = \left[-\left(F/\sqrt{\gamma}\right)y_\xi\right]\boldsymbol{i} + \left[\left(F/\sqrt{\gamma}\right)x_\xi\right]\boldsymbol{j} \tag{2.20}$$

acts on the membrane element.

The pressure included in eq. (2.19) is determined as follows: If the velocity–pressure formulation of the Navier–Stokes equations is used and they are evaluated on the membrane surface, where the velocity $\boldsymbol{u} = 0$ in a steady state, we have

$$p_x\boldsymbol{i} + p_y\boldsymbol{j} = \left(-\omega_y\boldsymbol{i} + \omega_x\boldsymbol{j}\right)/\mathrm{Re} \tag{2.21}$$

after using the continuity equation. Taking the scalar product of eq. (2.21) with $d\boldsymbol{r} = (dx)\boldsymbol{i} + (dy)\boldsymbol{j}$ and changing the variables to the transformation variables, we have

$$dp = (1/J\mathrm{Re})\left(\beta\omega_\xi - \gamma\omega_\eta\right) d\xi, \tag{2.22}$$

where $J = x_\xi y_\eta - x_\eta y_\xi$ and $\beta = x_\xi x_\eta + y_\xi y_\eta$. Integrating this equation along the membrane surface, we have the pressure distribution on the surface.

The length of the membrane L_M is calculated by eq. (2.18) and is given by

$$L_M = L_M^*/L = \int_{\xi_1}^{\xi_L} \sqrt{\gamma}\, d\xi, \tag{2.23}$$

where ξ_1 and ξ_L correspond to the edges of the membrane.

2.4. Drag on the membrane

The drag acting on the membrane may be calculated by integrating the stresses along the membrane surface. The vorticity and hence the shear stress at the edges of the membrane, however, will be very large. This causes a large numerical error in drag calculation using the stress along the membrane. Instead, we apply the momentum theorem to a control surface C enlosing the membrane. Then, the drag coefficient C_D can be calculated by the following formula:

$$\begin{aligned} C_D = \frac{(\mathrm{drag})}{\rho U^2 L} = &-\frac{\partial}{\partial t}\int_C \psi x_\xi \, d\xi + \int_C \left(u^2 y_\xi - uv x_\xi\right) d\xi \\ &+ \int_C \left\{ p y_\xi - (2/J\mathrm{Re})\left(y_\eta u_\xi - y_\xi u_\nu\right) y_\xi \right. \\ &\left. + (1/J\mathrm{Re})\left[\left(x_\xi u_\eta - x_\eta u_\xi\right) + \left(y_\eta v_\xi - y_\xi v_\eta\right)\right] x_\xi \right\} d\xi. \end{aligned} \tag{2.24}$$

In the actual calculation, we shall let the surface C coincide with the line $\eta = 6$, which is the sixth curve from the membrane (cf. fig. 2b).

3. Numerical calculation

Though we are interested in the steady state of the flow, we shall obtain it as a solution of an initial value problem. The time dependent method is especially effective in the present problem, because the membrane shape is easily adjustable so that the forces on the membrane element may be balanced in its equilibrium state. We employ a finite difference scheme to solve the differential equations concerned. Most space derivatives are approximated by the second-order central differences and some derivatives at boundaries by the second-order backward or forward differences. The first-order backward difference is used for time derivative. The time step size for all cases of the Reynolds number is taken to be 0.001.

It is preferable to specify the outer boundary conditions far away from the membrane, but actually we must be satisfied with a finite distance from the membrane. The outer boundary is taken as a circle of radius $r_{\max}$, whose value is shown in table 1. We use the uniform flow condition (2.7) on the upstream boundary, while on the downstream boundary we take

$$\omega_{xx} = 0, \quad \psi_{xx} = 0. \tag{3.1}$$

At the membrane surface, eq. (2.8) leads to

$$\psi_{i,1} = 0, \tag{3.2}$$

where $\psi_{i,j} = \psi(\xi = i, \eta = j)$, and i and j indicate the mesh point (i, j) in the (ξ, η) plane. The vorticity must be specified at the membrane surface to solve the vorticity transport equation (2.1). The tangential velocity is not generally zero for an arbitrary distribution of the surface vorticity. Zero tangential velocity may be attained using an iteration method. That is, we take

$$(\omega_{i,1})^{k+1} = (\omega_{i,1})^{k} - \frac{(V_{i,1})^{k}\left[(\omega_{i,1})^{k} - (\omega_{i,1})^{k-1}\right]}{(V_{i,1})^{k} - (V_{i,1})^{k-1}}, \tag{3.3}$$

where $V_{i,1}$ is the tangential surface velocity and the superscript k denotes the iteration number.

The algorithm for the numerical calculation is as follows:

(1) Assume an initial shape of the membrane under a given tension T_0 at its fixed ends and calculate the corresponding body-fitted coordinates.

(2) Assume the initial stream function and vorticity.

(3) Obtain the distribution of vorticity by solving eq. (2.1) in the finite difference form with the successive underrelaxation method.

(4) Calculate the stream function satisfying eq. (2.2) with ω obtained in step (3).

(5) The procedures (3) and (4) are repeated until the non-slip condition (2.8) is satisfied.

(6) Calculate the force acting on a membrane element. If the equilibrium condition (2.19) is not satisfied, modify the membrane shape according to the force $\boldsymbol{F}$ (see eq. (2.20)).

(7) Step the time increment forward, compute a new body-fitted coordinate system and return to step (3).

Table 1
Parameters used in numerical calculations.

Re	$r_{\max}$	$i_{\max}$	$j_{\max}$
5	20	50	80
10	10	50	50
20	10	50	50

(8) The above procedure will be repeated until the equilibrium condition at the membrane element is satisfied and the steady state is obtained.

4. Results and discussion

Numerical calculations were carried out for Reynolds numbers Re = 5, 10 and 20. In each case, the computation started from the case of a flat plate which corresponds to infinite tension force. The stream lines and the equivorticity lines obtained for a flat plate when Re = 5, 10 and 20 are compared with the results by Hudson and Dennis (1985). Figures 4a, 5a and 6a show the stream lines (upper half) and the equivorticity lines (lower half). The dotted

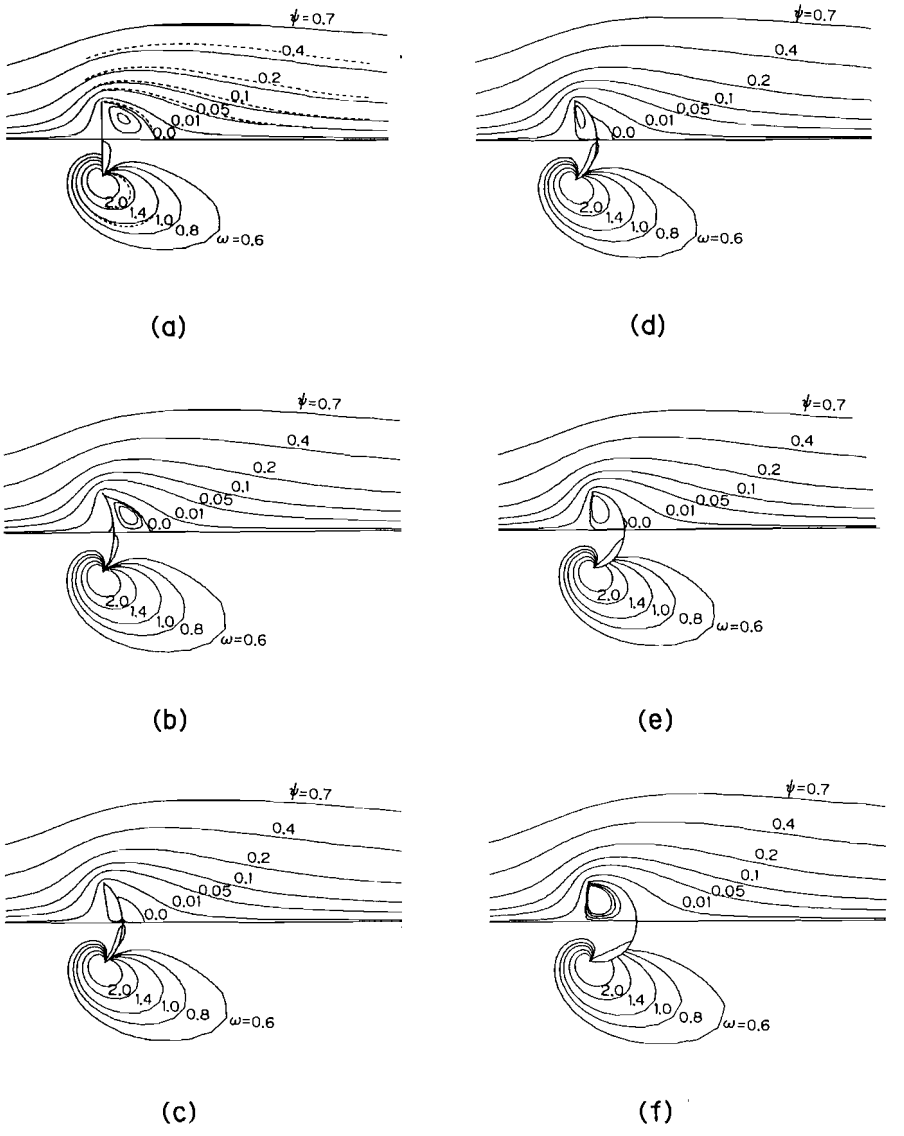

Fig. 4. Flow patterns and equivorticity lines at Re = 5. (a) $T_0 = \infty$, (b) $T_0 = 1.5$, (c) $T_0 = 1.12$, (d) $T_0 = 1.06$, (e) $T_0 = 1.03$, (f) $T_0 = 1.12$.

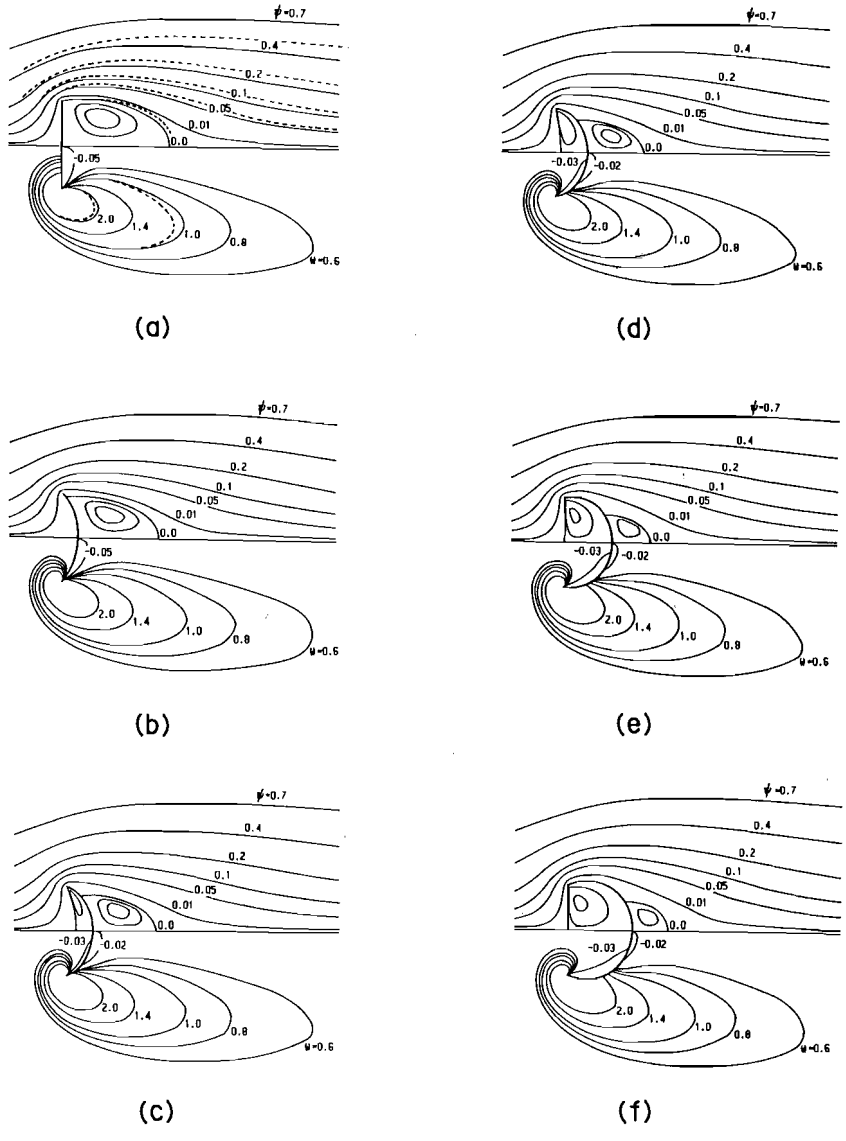

Fig. 5. Flow patterns and equi-vorticity lines at Re = 10. (a) $T_0 = \infty$, (b) $T_0 = 1.0$, (c) $T_0 = 0.8$, (d) $T_0 = 0.769$, (e) $T_0 = 0.836$, (f) $T_0 = 0.928$.

lines are drawn from Hudson and Dennis. It is seen that the agreement of both results are not so bad.

Figure 4 shows the flow fields when Re = 5. The flow is separated at the edges of the membrane and there are two eddies on the backside of the membrane when $T_0 = \infty$. The membrane becomes convex to the right and the separation points move towards middle as the tension decreases. There appear additional twin vortices on the concave side of the membrane when the tension decreases to 1.12. As the tension decreases further, the membrane becomes more concave and the twin vortices on the rear decrease in size. However, we cannot get an equilibrium shape when the tension is smaller than about 1.03. Therefore, we must increase the tension strength in order to get a more concave shape in equilibrium. Figure 4f shows this flow pattern. This means that the tension has a critical value below which there is

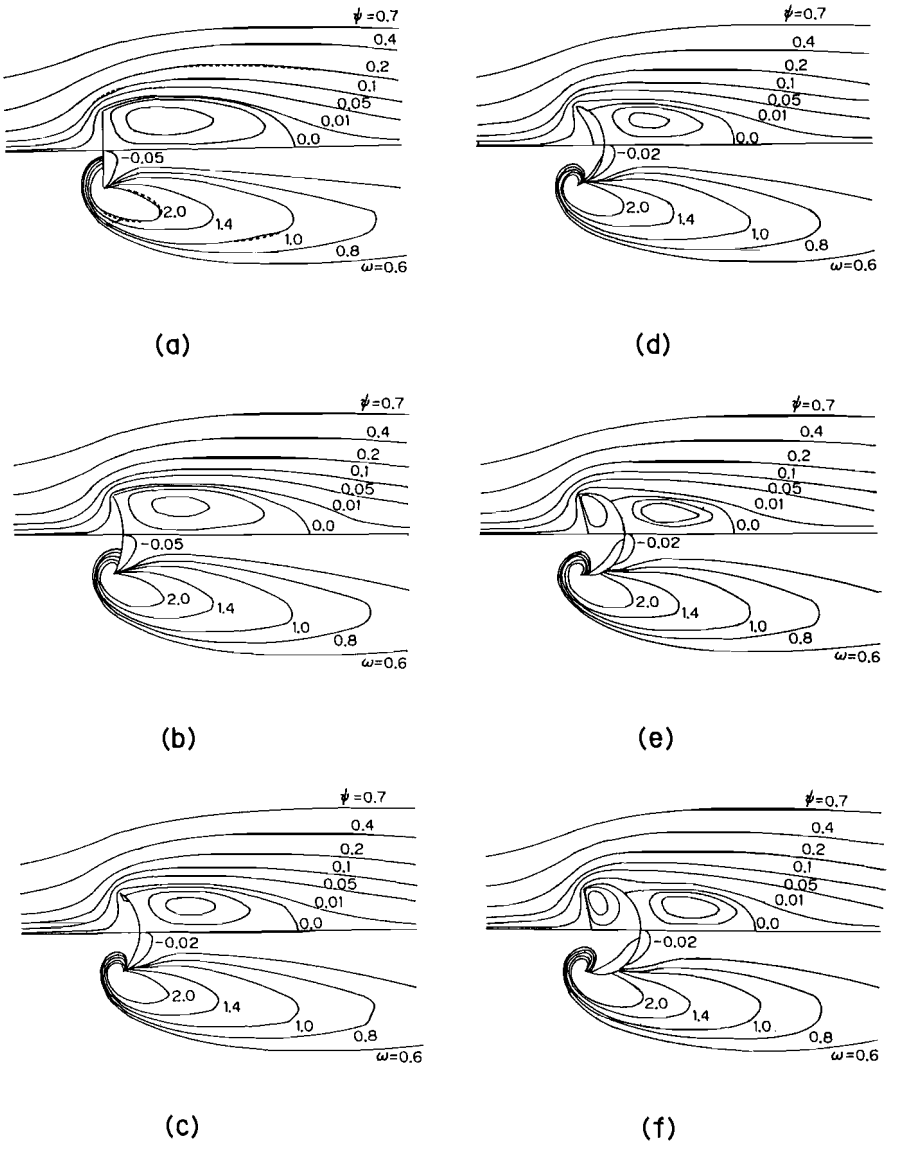

Fig. 6. Flow patterns and equi-vorticity lines at Re = 20. (a) $T_0 = \infty$, (b) $T_0 = 1.0$, (c) $T_0 = 0.6$, (d) $T_0 = 0.561$, (e) $T_0 = 0.62$, (f) $T_0 = 0.707$.

no shape of the membrane in equilibrium. Above the critical value, we have two different kinds of flow at one membrane tension, i.e. corresponding to two different concavities of the membrane. We shall understand why there is a minuimum value of the tension if we consider two extreme cases, i.e. the flows past a flat membrane and a highly concave shape. The tension is obviously infinite in a flat membrane; in the case of a highly concave membrane, the tangential force acting on the membrane will be very large because the membrane length is very long, resulting in large tension. Therefore, the tension first decreases and then increases as the membrane shape is distorted between these two extreme cases. It is interesting to see in figs. 4e and 4f that the twin eddies on the front side are almost enclosed within the region between the membrane and the straight joining its edges.

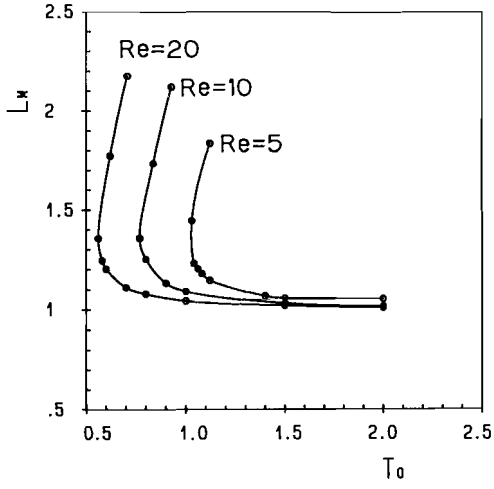

Fig. 7. Membrane length versus membrane tension.

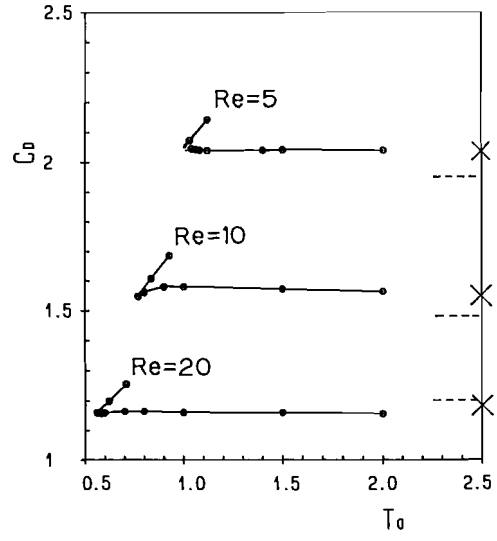

Fig. 8. Drag coefficient versus membrane tension.

The behavior of the flow at other Reynolds numbers is also similar to that for Re = 5, if the changes in the membrane tension follow the same trend (see figs. 5 and 6). The critical value of the non-dimensional membrane tension below which we cannot get the equilibrium shape decreases with increasing Reynolds numbers. The critical values of the tension obtained are about 0.769 and 0.561 for the Reynolds numbers of 10 and 20, respectively.

The variation of the membrane length versus tension is shown in fig. 7 for each Reynolds number. It will be seen from this figure that the length gradually increases from that of flat plate as the tension decreases. Once the critical value of the tension is reached, the length increases greatly and alomost linearly as the tension increases again. It is interesting to see that there is no equilibrium membrane shape below the critical point and that the variation of the length with the tension is very large after the critical point. The membrane has two different shapes for one tension.

Figure 8 shows the variation of the drag acting on the membrane versus the tension for each value of the Reynolds number. It is interesting to note that the drag is almost constant and has a value close to that of a flat plate, which is shown as a cross, as the tension decreases

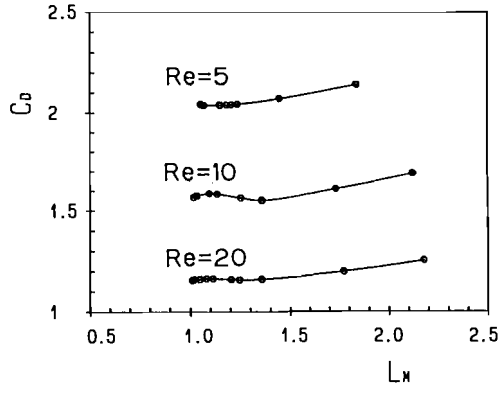

Fig. 9. Drag coefficient versus membrane length.

from infinity to the critical value. Then, the drag increases almost linearly as the tension increases. The comparison is made with the drag of the flat plate obtained by Tamada, Miura and Miyagi (1983). Their formula is valid for Re less than about 5. We plot their drag in fig. 8 as the dotted lines by simply extrapolating their curves to higher Reynolds numbers. It is seen that the relative errors between both results are of the order of several per cent. We can calculate the drag on the membrane of a given length by using figs. 7 and 8. Figure 9 shows the plot of the drag versus the length of the membrane.

References

Hudson, J.D. and S.C.R. Dennis (1985) The flow of a viscous incompressible fluid past a normal flat plate at low and intermediate Reynolds numbers: the wake, *J. Fluid Mech. 160,* 369–383.

Lee, S.H. and L.G. Leal (1982) The motion of a sphere in the presence of a deformation of a sphere normal to an interface, *J. Coll. Interf. Sci. 87,* 81–106.

Miksis, M., J.M. Vanden-Broeck and J. Keller (1981) Axisymmetric bubble or drop in a uniform flow, *J. Fluid Mech. 108,* 89–00.

Nielsen, J.N. (1963) Theory of flexible aerodynamic surface, *ASME J. Appl. Mech. 30,* 435–442.

Ryskin, G. and L.G. Leal (1984) Numerical solution of free-boundary problems in fluid mechanics, Part 1. The finite-difference technique, *J. Fluid Mech. 148,* 1–17.

Shanks, S.P. (1977) Numerical simulation of viscous flow about submerged arbitrary hydrofoils using non-orthogonal, curvilinear coordinates, *Ph.D. Dissertation,* Mississippi State University.

Sugimoto, T. and J. Sato (1988) Aerodynamic characteristic of two-dimensional membrane airfoils, *J. Japan Soc. Aero. space Sci. 36,* 86–93 (in Japanese).

Tamada, K., H. Miura and T. Miyagi (1983) Low-Reynolds-number flow past a cylindrical body, *J. Fluid Mech. 132,* 445–455.

Thwaites, B. (1961) The aerodynamic theory of sails I, *Proc. R. Soc. A 261,* 402–422.

Thompson, J.F., F.C. Thames and C.W. Mastin (1974) Automatic numerical generation of body-fitted curvilinear coordinate system for field containing any number of arbitrary two-dimensional bodies, *J. Comput. Phys. 15,* 299–319.

Yamamoto, K. and K. Ishimaru (1988) Oscillation of a sail in a flow, *J. Japan Soc. Aerno. Space Sci. 36,* 233–241 (in Japanese).

Youngren, G.K. and A. Acrivos (1976) On the shape of a gas bubble in a viscous extensional flow, *J. Fluid Mech. 76,* 433–442.

Zahalak, G.I., P.R. Rao and S.P. Sutera (1987) Large deformations of a cylindrical liquid-filled membrane by a viscous shear flow, *J. Fluid Mech. 179,* 283–305.